A DFT/TD-DFT Study on Pyridine-Anchored Schiff Base Molecules for DSSC Applications

Melike AYAZ [iD], Yusuf ERDOGDU* [iD]

Science Faculty, Department of Physics, Gazi University, 06400, Teknikokullar, Ankara, Türkiye

Highlights
• It has been designed to illustrate the energy diagram of the dyes, TiO_2, and electrolyte.
• DFT and TD-DFT methodologies were employed to explore the designed photosensitizers.
• Predictions were made for the photovoltaic, electrical, and optical properties of the dyes.

Abstract

The primary objective of this research is to examine the Schiff bases produced from pyridine-anchored molecules, with a specific focus on their potential utilization in dye-sensitized solar cells (DSSCs). The electrical, spectroscopic, and photovoltaic properties of dyes incorporating a pyridine anchor were calculated utilizing DFT and TD-DFT methodologies. The geometries, electronic characteristics, and photovoltaic properties of the dyes under investigation were evaluated using DFT-B3LYP/6-311++G(d,p) quantum chemical simulations. The excitation energies and UV-Vis spectra of the dyes have been computed utilizing the TD-DFT-B3LYP/6-311++G(d,p) methodology and the conductor-like polarizable continuum model (C-PCM). The electron injection and dye regeneration processes are contingent upon the energy levels of the highest occupied molecular orbital (HOMO) and lowest unoccupied molecular orbital (LUMO) of these dyes. The investigation focused mainly on four fundamental components exhibiting robust interconnections and equivalent significance: light-harvesting efficiency (LHE), electron injection free energy (ΔG^{inject}), and reorganization energy. The determined HOMO energy levels are observed to be lower than the redox potential, indicating that the suggested dyes possess the capability to acquire electrons from redox and successfully undergo dye regeneration. Furthermore, the LUMO of the dyes exhibits a more significant negative energy level in comparison to the conduction band of TiO_2. Thus, it demonstrates that the transfer of electric charge from the LUMO level to TiO_2 is thermodynamically favorable. The more considerable negative ΔG^{inject} value obtained by calculation suggests that Dye-1 may have a higher ability to inject charge.

1. INTRODUCTION

The increasing global energy demands have led to significant international interest in utilizing DSSCs to address them in an environmentally sustainable manner [1]. These devices, which convert light into electricity, possess distinctive characteristics such as affordability, simplicity in production, high efficacy, flexibility, lightweightness, multicolor capability, and transparency. These attributes are achieved by utilizing photosensitizers that adsorb onto the surfaces of mesoporous films composed of TiO_2 nanocrystals [2]. In recent years, substantial gains in the power conversion efficiency (PCE) of DSSCs have been made due to innovative material design and substantial device engineering efforts [3]. Including a sensitizer in a solar cell is of utmost importance as it plays a pivotal role in dictating the photovoltaic properties of the device, including charge separation, charge recombination, and light absorption [4–8]. The classification of sensitizers can be broadly categorized into three groups: natural dyes, metal-containing complex dyes, and organic dyes.

---

*Corresponding author, e-mail: yerdogdu@gazi.edu.tr

Complex molecules containing metals exhibit substantial efficacy in solar energy applications. One of the most important sensitizers used in DSSC applications is Ru(II) metal complexes. The high photo conversion efficiency of ruthenium (II) metal-based dyes has resulted in their application as sensitizers in DSSCs. Extensive research has been conducted on the ruthenium (II) polypyridyl compound. The remarkable stability and unique redox characteristics of ruthenium (II) metal-based dyes are crucial factors that allow their utilization in DSSCs. Despite being a favored option for sensitizing DSSCs, the use of ruthenium dye presents notable disadvantages, including the adverse effects of heavy metal toxicity, high costs, challenges associated with maintaining purity, and the requirement for intricate synthesis techniques. Employing alternative metal-free replacements for ruthenium complex dyes as sensitizers may offer a feasible resolution to these issues [9-12]. Ruthenium complexes represent exemplary instances of metal-containing dyes. Consequently, researchers have directed their attention towards advancing organic sensitizers due to their abundant accessibility, cost-efficiency, and remarkable light-capturing capabilities. Organic dyes possess notable attributes, including a substantial molar extinction coefficient and the capacity to modify their chemical structure [13]. The essential constituents of these sensitizers consist of donor (D), π-bridge (π), and acceptor (A) moieties. The D-π-A configuration, distinguished by a push-pull structure, has been known for its ability to enhance power conversion efficiency and facilitate efficient load transfer [14]. By manipulating the D, π, and A components of dyes, it becomes feasible to effectively alter their absorption spectra, along with the energy levels, linked to the HOMO and LUMO. Recently, considerable advancements have been achieved in augmenting the efficacy of DSSCs through the exploration and implementation of diverse approaches that enable the effective utilization of organic dyes. The dyes referenced in the passage demonstrate diverse photophysical, electrochemical, and other characteristics, rendering them appropriate for utilization as sensitizers in DSSCs [15]. The primary focus lies in the robust capacity of electron donors to transfer electrons [16]. The electron-donating ability of the donor components, the electron-accepting ability of the acceptor components, and the pi bridge are the factors that determine the photophysical, electrochemical, and ICT properties of D-π-A dyes [17]. Efficient electron transfer is achieved through the directional movement of electrons from HOMO to LUMO.

The structural composition of organic dyes plays a pivotal role in influencing the efficiency and effectiveness of DSSCs. To achieve high power conversion efficiency (PCE), this structure must demonstrate the following key characteristics: The objective is to attain a suitable arrangement of the Highest Occupied Molecular Orbital (HOMO) and Lowest Unoccupied Molecular Orbital (LUMO) energies, enabling effective electron injection and dye renewal. Furthermore, it is crucial to possess an absorption band that includes a broad spectrum of visible and near-infrared light wavelengths to optimize the efficacy of light capture. Additionally, it is imperative to have a robust conjugation among dye molecules to facilitate efficient Intramolecular Charge Transfer (ICT) [18, 19].

Applying a theoretical framework in examining sensitizers has proven to be a highly effective method for cost reduction, minimizing delays, and reducing errors in experimental investigations [20,21]. The utilization of Density Functional Theory (DFT) and Time-Dependent Density Functional Theory (TD-DFT) calculations was employed to carry out optimization and determine the photophysical properties. Our work [22] involved examining the electronic properties and absorption spectra of the generated dyes. An Acceptor-Donor-π-Acceptor (A-D-π-A) design was utilized to fabricate a unique organic DSSC. The pyridine group was identified as the electron acceptor (A), while the phenyl and N-CH3 groups were determined to serve as the electron donors (D). Examining these sensitizers includes the evaluation of frontier molecular orbitals, absorption spectra, light harvesting efficiency, molar extinction coefficient, electron injection, and regeneration.

2. COMPUTATIONAL DETAILS

Utilizing a theoretical framework for examining sensitizers has proven highly effective in managing expenses, minimizing time constraints, and reducing inaccuracies in empirical investigations. The dye compounds underwent quantum mechanical simulations using the Gaussian 09W (Revision B.01) program. The force gradient approach, implemented with Berny's algorithm and conventional convergence criteria for geometry optimization, was employed to fully optimize the molecular geometries. The calculations were executed using default convergence criteria, without limitations on geometry [23]. This study delved into

the spectroscopic, electrical, and photophysical characteristics of dye molecules. The DFT-B3LYP/6-311G++(d,p) method was employed [24–26]. The absorption characteristics of the dye molecules within the wavelength range of 0-700 nm were determined using the C-PCM method, employing TD-DFT computations. Extensive research, both experimental and theoretical, has been conducted to explore the computation of electrical characteristics, vertical excitation energy, and optical absorption spectra [27-29]. However, the precision of these computations is significantly influenced by the choice of functional employed for charge transfer excitations. The researchers employed four distinct functionals to determine the most suitable one for this investigation. The computations were conducted using the B3LYP/6-311++G(d,p), M06-2X/6-311++G(d,p), wB97XD/6-311++G(d,p), and CAM-B3LYP/6-311++G(d,p) functionals [30-32].

The words "E^{dye}" and "E^{dye*}" were identified by computational research employing the B3LYP functional. The terms "E^{dye}" and "E^{dye*}" represent the oxidation potential of the ground and excited states, respectively. Furthermore, determining ΔG^{inject}, LHE, and lifetime (τ) involved the consideration of the oscillator strength (f) of dye molecules at their maximum absorption. The computations were conducted in accordance with other research investigations [33, 34]. The aforementioned equations have been utilized to calculate the photovoltaic characteristics. The transport of electrons from the dye in an excited state to the semiconductor layer depends on the transition of the first excited state to the ground state. A prolonged period in the excited state enhances the facilitation of charge transfer from the dye to the semiconductor. The formula provided was utilized to ascertain the anticipated duration of the dye's excited condition. The f relates to the electronic state, whereas E_{exc} indicates the excitation energy corresponding to each unique electronic state.

DFT and TD-DFT calculations were utilized to conduct optimization and determine photophysical properties. In this work, we have evaluated the electronic properties and absorption spectra of the designed dyes. The D-π-A design was utilized to fabricate an organic DSSC. The pyridine group was responsible for fulfilling the role of the electron acceptor, whereas the phenyl and N-CH$_3$ groups were attributed to the function of the electron donor. Examining these sensitizers includes the evaluation of frontier molecular orbitals, absorption spectra, LHE, molar extinction coefficient, electron injection, and dye regeneration [35]

$$E^{dye} = -E_{HOMO} \tag{1}$$
$$E^{dye*} = E^{dye} - E_{exc} \tag{2}$$
$$\Delta G_{inject} = E_{dye*} - E_{CB} \tag{3}$$
$$\Delta G_{reg} = ((E_{I_3^-/I^-}) - E_{HOMO}) \tag{4}$$
$$\tau = \frac{1.499}{fE^2} \tag{5}$$
$$LHE = 1 - 10^{-f} \tag{6}$$

Furthermore, the global hardness (η), ionization potential (IP), and electron affinity (EA) were computed using the functional and basis sets mentioned in the previous statement [36] The features of compounds are obtained by utilizing the corresponding formula, which takes into account the ground state IP and EA. The capacity of a structure to accept electrons is denoted by its chemical potential (μ) and electrophilic index (ω). A strong electrophilic nature is associated with elevated chemical potential and electrophilicity index values [37]. The term electrophilicity power (ω) denotes the amount of energy required to restore equilibrium in a system that has acquired excess electronic charge from its surroundings. To predict the abilities of chemical species to donate or take electrons, Gazquez and colleagues [38] proposed the introduction of two novel metrics, namely electron-donating power (ω^-) and electron-accepting power (ω^+). The related equations of the parameters are given in the references [36, 37].

In this study, we also computed the molecular reorganization energies described in the following equations. Our investigation is limited to the computation of molecular reorganization energy, characterized by the terms outlined in reference [39]. The value of Λ_{total} is obtained by adding together the reorganization energy associated with the movement of electrons (Λ_e) and holes (Λ_h). The variables Λ_e, Λ_h, and Λ_{total} were computed utilizing the subsequent equations

$$\Lambda_e = (E_n^- - E_a) + (E_a^0 - E_n) \tag{13}$$

$$\Lambda_h = (E_n^+ - E_c) + (E_c^0 - E_n) \tag{14}$$
$$\Lambda_{total} = \Lambda_e + \Lambda_h. \tag{15}$$

The term "E_n" refers to the energy level that is most favorable for the neutral state, "E_c" indicates the energy level that is optimized for the cationic state, and "E_a" designates the energy level that is optimized for the anionic state. The variables E_n^+ and E_n^- denote the individual point energies of the cation and anion, respectively, while preserving their neutral geometric configuration. Similarly, the symbols E_c^0 and E_a^0 are used to represent the single point energies of the neutral state, with the cationic and anionic geometries remaining unaltered. In this study, the molecular rearrangement energies described in the subsequent equations were also calculated. The scope of our inquiry is restricted to calculating molecular rearrangement energy, as defined by the nomenclature outlined in reference [39].

3. RESULTS AND DISCUSSION

3.1. Molecular Structure and Dipole Moment

The atomic numbering and molecular geometry of the dyes under investigation are depicted in Figure 1. Table 1 summarizes the molecular structural features of the dyes under investigation. There exists a positive correlation between the molecular planarity of a dye and the degree of photoinduced electron injection into the CB of a semiconducting surface. The charge species within planar dye molecules exhibit delocalization, elongating the dye's charge separation lifespan. Table 1 presents the dihedral angles that exhibit planarity. Research findings have provided evidence to support the notion that the planarity of all dyes is highly similar. The excited state dipole moment (μ_e) and ground state dipole moment (μ_g) of the dyes under investigation were determined and are presented in Table 1. The comparative analysis of the dipole moments of various dyes, as presented in Table 1, reveals that Dye-1 exhibits a greater dipole moment than the other dyes. High dipole moment data suggests that the dye molecule has polarity. The dipole moment values in the excited state demonstrate an increase in magnitude compared to those observed in the ground state. Upon analysis of the above data, it is evident that the excited states manifest a greater level of polarity when contrasted with the ground state.

Table 1. The dihedral angles and dipole moments of the dyes

	φ_1 (Å)	φ_2 (Å)	μ_g (Debye)*	μ_e (Debye)**
Dye-1	26.13	9.18	6.337	25.92
Dye-2	27.55	12.31	4.432	24.72
Dye-3	24.63	12.25	2.440	21.80

*Ground state
**Excited state
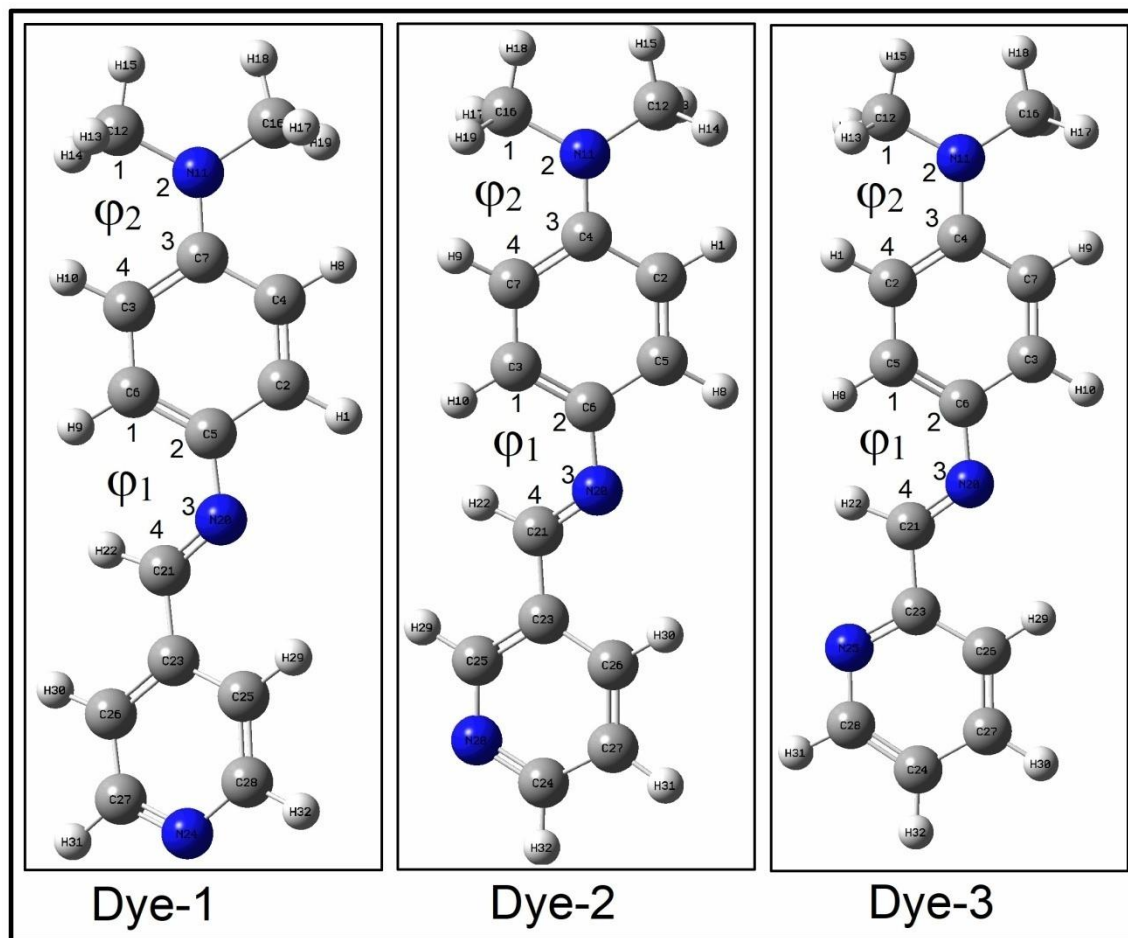
Figure 1. *The molecular structure of the dyes, together with the corresponding atomic numbering*

3.2. UV-Vis Spectra

The absorption characteristics of the dyes were acquired to assess their photophysical properties. Table 2 presents the pertinent features. Figures 2, 3, and 4 depict the absorption of the dye in the chloroform solvent within the visible area. Upon examination of the UV spectra presented in Figure 2-4, it can be inferred that the dyes possess the capacity to serve as photosensitizers for DSSCs. he wavelengths at which Dye-1, Dye-2, and Dye-3 exhibit their highest absorption peaks (λ_{max}) are 443.52 nm, 433.84 nm, and 429.01 nm, respectively. Akdogan et al. [11] observed the experimental UV-Vis spectra at a wavelength of 388 nm for the synthesized dye. Theoretical UV-Vis spectrum analysis revealed that Dye-1, Dye-2, and Dye-3 had higher wavelength peak values compared to the synthesized dye. The transition from the HOMO to the LUMO in electronic systems, specifically with a 70% configuration, results in the formation of an excited state denoted as the transition from the ground state (S_0) to the first excited state (S_1). The order of increasing f values for the dyes is as follows: Dye-2 (0.6666) < Dye-1 (0.7164) < Dye-3 (0.75590).

The estimated peak absorption wavelengths for Dye-1 were found to be 430.4 nm (B3LYP), 423.3 nm (CAM-B3LYP), 427.4 nm (M06-2X), and 422.1 nm (wB97XD). When there is an increase in the percentage contribution of the change in functional HF quantity, it is anticipated that the maximum absorption will shift towards the blue region. Here, a decrease in ultraviolet-visible (UV-Vis) spectrum absorption is observed. The B3LYP functional exhibited the highest absorption value due to its minimal contribution to the overall percentage change in the HF component within the functional. The B3LYP functional gives more reasonable band gap energy than the long-range corrected density functional theory (LC-DFT) functional, while the LC-DFT functional for the absorbance of photoexcitations is more precise than that of the B3LYP functional [40-43].
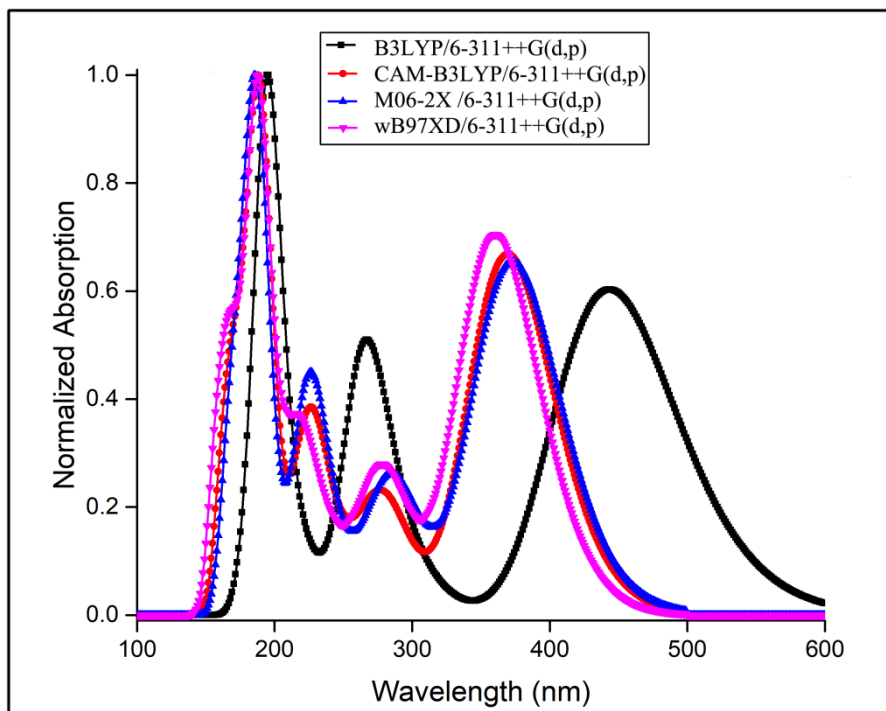
Figure 2. *The theoretical UV-Vis spectra of the Dye-1*
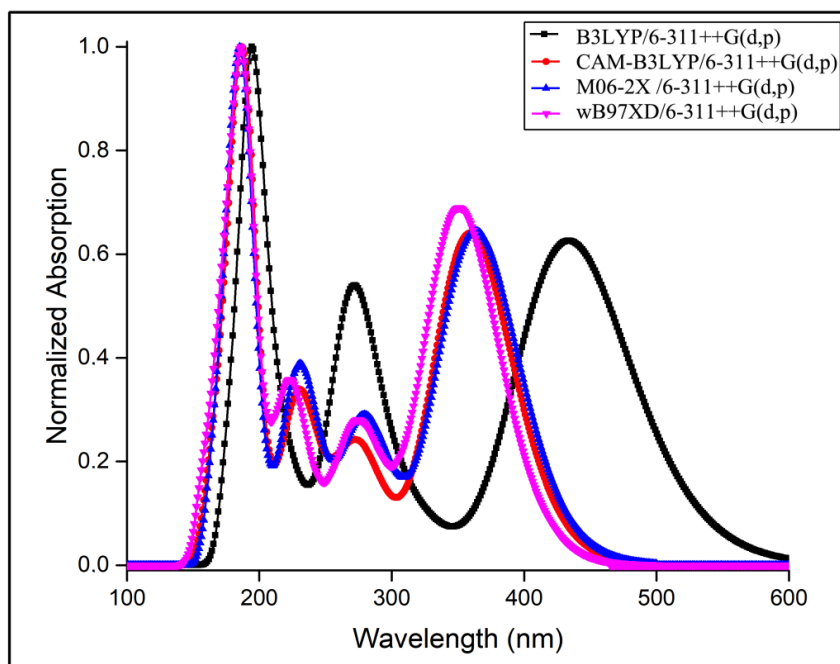
Figure 3. *The theoretical UV-Vis spectra of the Dye-2*
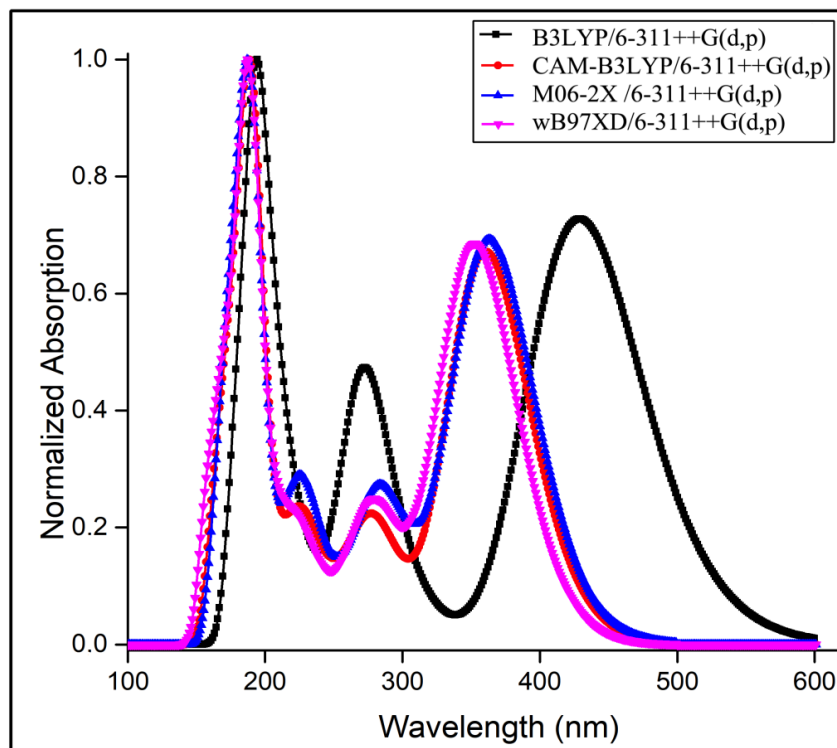
Figure 4. *The theoretical UV-Vis spectra of the Dye-3*

Table 2. *The UV-Vis spectral data of the dyes*

	Dye-1	Dye-2	Dye-3
Wavelength λ(nm)	443.52	433.84	429.01
Excitation energies (eV)	2.7954	2.8579	2.8900
Oscillator strengths (*f*)	0.7164	0.6666	0.7559
Excited state	HOMO LUMO(70%)	HOMO LUMO(70%)	HOMO LUMO(70%)
ε (x10^4 $M^{-1}cm^{-1}$)	2.9	2.7	3.06

3.3. The Energy Levels and Gaps

The outputs for HOMO, LUMO, and their energy gap (E_{gap}) are presented in Table 3. These values were obtained using the B3LYP/6-311++G(d,p) computational method. The HOMO energy levels were determined to be -5.418 eV (for Dye -1), -5.312 eV (for Dye-2), and -5.261 eV (for Dye-3). The observed energy levels are ascertained to be below the potential of I^-/I_3^- (-4.8 eV), recommending that the proposed dyes possess the ability to receive electrons from I^-/I_3^- and potentially undergo effective reduction and regeneration, as demonstrated in Figure 5. The LUMO of dyes has a greater negative energy level in comparison to the conduction band of TiO_2, specifically measuring -4.0 electron volts (eV). The aforementioned suggests that the transport of charge from the LUMO level to TiO_2 is highly effective and exhibits thermodynamic favorability, as demonstrated in Figure 5.

Table 3. *The energies of HOMO and LUMO for corresponding compounds*

	E_{HOMO}(eV)	E_{LUMO}(eV)	E_{H-L}(eV)
Dye-1	-5.418	-2.104	3.315
Dye-2	-5.312	-1.948	3.365
Dye-3	-5.261	-1.878	3.383

To enhance the LHE and facilitate the absorption of red-shifted light within the visible spectrum, it is imperative to cut the E_{gap} of the dyes. This reduction in E_{gap} indicates the transition energy associated with $\pi \rightarrow \pi^*$ electronic transitions. The E_{LUMO} of the dye molecules was determined and is presented in Table 3. The computed values were found to be -2.104eV (for Dye-1), -1.948eV (for Dye-2), and -1.878eV (for

Dye-3). The E_{HOMO} value is frequently employed as a metric to assess the electron-donating capacity of a molecule, while the E_{LUMO} value is utilized to quantify its electron-accepting capability. The kinetic stability and chemical reactivity of dye molecules are determined by the frontier orbital gaps. Molecules that possess frontier orbital gaps of relatively small magnitudes are frequently associated with diminished kinetic stability and heightened chemical reactivity. The analysis reveals that Dye-1 exhibits the lowest level of softness, while Dye-3 demonstrates the highest degree of hardness. Dye-1 has a significantly elevated level of chemical reactivity in comparison to the remaining dyes.

Akdogan et al. estimated the energy levels of the produced dye to be -6.188 eV for HOMO and -2.611 eV for the LUMO [11]. The synthesized dye demonstrates a HOMO energy that is roughly 0.7-0.9 eV lower than Dye-1, Dye-2, and Dye-3. The synthesized dye has a LUMO energy of approximately 0.5-0.7 eV lower than that of Dye-1, Dye-2, and Dye-3. The experimentally measured PCE value of the synthesized dye is 0.47.
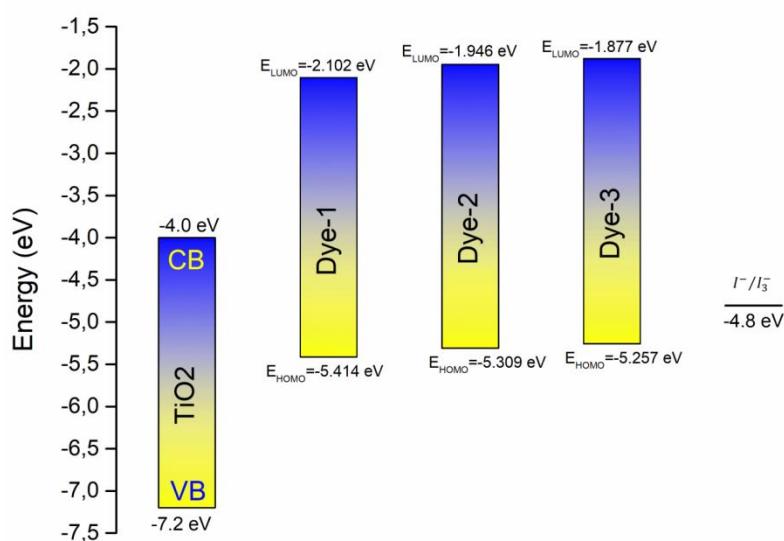
Figure 5. *The energy levels of the HOMO and LUMO for both the dyes and TiO₂*

3.4. Frontier Molecular Orbitals

The molecular orbitals of the dyes are depicted in contour maps presented in Figure 6. In the HOMO, electron dispersions are uniform across the molecule, with significant concentrations observed in the phenyl, N-CH3, and π-linkers. Similarly, the LUMO distributes its electrons throughout the molecule, with most found in the pyridine group and the π-linkers.
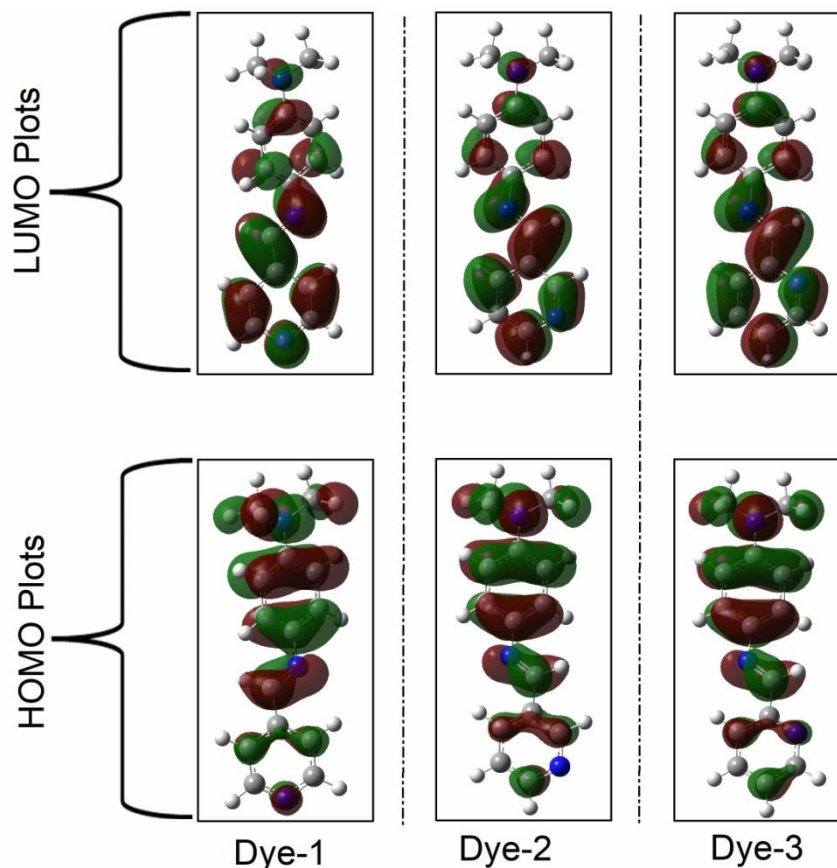
Figure 6. *The plots of the HOMO and LUMO for the dyes*

Using the Multiwfn software [44], various maps were generated, including charge density difference maps (CDDM) depicting the disparity between excited and ground states, maps illustrating the distribution of holes and electrons, and C_{hole}/C_{ele} function maps. Additionally, significant parameters such as the hole and electronic degree of overlap index (S_r) and the center of mass distance index (D) were calculated and are presented in Table 4.

The density of the excited state in the CDDM shows a rise in the blue region and a decline in the green region, corresponding to the density of the ground state. This illustrates the process of transferring charge from the electron-donating group to the electron-attracting group using π-linkers. The C_{hole}/C_{ele} function maps employ blue to represent the hole distribution and green to represent the electron distribution. As the Sr index decreases, the degree of hole and electron separation becomes more pronounced. The Sr index values for Dye-1, Dye-2, and Dye-3 were determined to be 0.584, 0.580, and 0.595 respectively. Despite Dye-2 being comparatively smaller, its Sr index values were found to be close together. The hole and electron separations of Dye-2 are more sufficient than those of the other two dyes, as evidenced by its smaller Sr index in Table 4.

Table 4. *The distribution maps of* ^{a}*CDDM, holes, and electrons, as well as the maps of* C_{hole}/C_{ele} *function,* ^{c}D *and* ^{d}Sr

	^{a}CDDM	^{b}HoleandElectron	^{b}C$_{hole}$andC$_{ele}$	^{c}D(Å)	^{d}S$_{r}$
Dye-1				4.189	0.584
Dye-2				4.306	0.580
Dye-3				4.107	0.595
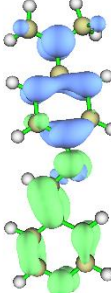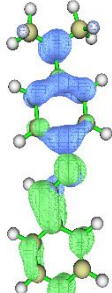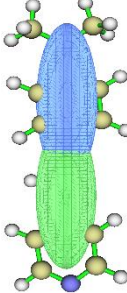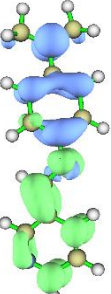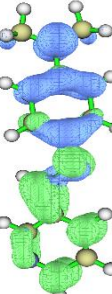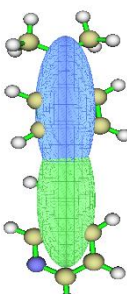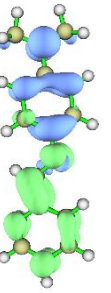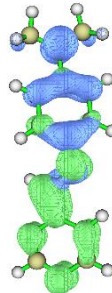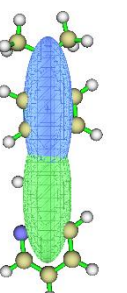
3.5. Photovoltaic Parameters

The outcomes, obtained through the utilization of relevant equations, are succinctly presented in Table 5. It is anticipated that to enhance the Power Conversion Efficiency (PCE) of a solar cell or improve the performance of a dye sensitizer, a negative ΔG^{inject} value and a positive ΔG_{reg} value will be present. All the sensitizers in Table 5 have negative ΔG^{inject} and positive ΔG_{reg} values. Dye regeneration occurs by reducing the oxidized dye molecule through the removal of an electron from a redox pair [45]. The ΔG_{reg} was predicted as 0.618 eV > 0.512 eV > 0.461 eV for the dyes Dye-1, Dye-2, and Dye-3 respectively. For DSSCs to operate at high efficiency, a low regenerative driving force is required because high driving forces are linked to photovoltage loss [46].

In the present work, it is demonstrated that the dye molecules exhibit a negative ΔG^{inject} value in the order of -1.377 eV (Dye-1) > -1.545 eV (Dye-2) > -1.629 eV (Dye-3). This observation suggests that the energy levels associated with the excited state are situated at a higher energy level compared to the Conduction Band (CB) of the semiconductor. As a result, it symbolizes an influx of electrons from the stimulated dye into the CB of TiO$_2$. The elevated J$_{SC}$ can be ascribed to the processes of dye renewal and fast electron injection. Due to their greater LUMO levels and more negative computed ΔG^{inject} values compared to Dye-2 and Dye-3, we surmised that they would have a significant capacity for charge injection because of a stronger driving force. Therefore, we hypothesized they might still exhibit considerable charge injection capability due to a stronger driving force.

Table 5. *The ΔG^{inject} and ΔG_{reg} of the dyes*

	Dye-1	Dye-2	Dye-3
E^{dye}(eV)	5.418	5.312	5.261
E^{dye*}(eV)	2.623	2.455	2.371
ΔG^{inject}(eV)	-1.377	-1.545	-1.629
ΔG^{reg}(eV)	0.618	0.512	0.461
τ(ns)	4.12	4.23	3.65
LHE	80.8	78.5	82.5

The Light Harvesting Efficiency (LHE) associated with each dye molecule's absorption at the maximum wavelength can be determined using a formula that incorporates the efficiency factor (*f*) of the dye. According to the LHE values, which exhibit high and similar values ranging from 80.8 to 82.5, it can be observed that all dyes possess the ability to optimize the photocurrent response. To achieve a high J_{SC}, the LHE of the dye must be maximized to the greatest extent possible. Table 5 presents a comprehensive compilation of the computed durations of the excited states for the various dyes. In the case of Dye-2, the greatest duration observed for charge transfer is 4.23 nanoseconds, which confers a notable advantage.

3.6. Ionization Potential, Electron Affinity and Electrophilicity

Table 6. *IP, EA and η values of the dyes examined in this study*

	Dye-1	Dye-2	Dye-3
IP(eV)	6.710	6.604	6.548
EA(eV)	0.935	0.774	0,737
η(eV)	2.887	2.915	2.906
ω(eV)	2.530	2.335	2.283
ω^{+}(eV)	0.980	0.854	0.825
ω^{-}(eV)	4.802	4.544	4.468
E_b	0.519	0.507	0.493

To assess the effectiveness of electron transport and dye injection, IP and EA may be efficient. How firmly an electron is connected to the system's nuclear attractive field can be seen by looking at its ionization potential. The dye is more likely to give electrons when the IP is lower; for electron injection, a higher EA is beneficial. The parameter of global hardness (η) quantifies the degree of resistance exhibited by molecules towards intramolecular charge transfer. The parameter has been employed as an indicator of the overall stability of the system.

For a more thorough explanation of the molecular characteristics of dyes, the electron accepting power ($\omega+$), which represents a chemical system's capacity to accept a minute fraction of charge, and the electron donating power ($\omega-$), which represents a chemical system's capacity to release a minute fraction of charge, have been studied [47]. Table 6 includes a list of these parameters. The value represents the stabilization energy of the dyes. These dyes' levels declined in the following order: 2.530 (Dye-1), 2.335 (Dye-2), and 2.283 (Dye-3). Because it attracted electrons from the environment, the ω of Dye-1 value was larger than that of the other dyes, suggesting higher energy stability. The symbolized as $\omega+$, measures an object's ability to accept an electron from a donor. To attain a high J_{SC}, it is preferable to have a greater value of $\omega+$. The $\omega+$ values of the dyes increased in the range of 0.825 (Dye-3), 0.854 (Dye-2) to 0.980 (Dye-1), showing that Dye-1 had the largest electron-withdrawing ability and, consequently, a stronger ability to attract electrons from the dye's acceptor moiety.

According to the calculations, the binding energy (E_b) values for the molecules decrease in the following order: 0.519 eV (Dye-1) > 0.507 eV (Dye-2) > 0.493 eV (Dye-3). Dye-3 has the lowest E_b of all the molecules. Since lower Eb aids exciton dissociation by rupturing the coulombic forces between the hole and electron, the higher the charge transfer rate, the lower the binding energy. Because of this, among the compounds suggested for use in solar cells, Dye-3 is the molecule that can serve as the best acceptor molecule.

3.7. Reorganization Energy

Furthermore, the total reorganization energy (Λ_{total}), comprising the reorganization energy associated with holes (Λ_h) and the reorganization energy associated with electrons (Λ_e), can provide insights into the balance between electron and hole transport.

Table 7. *The reorganization energy of holes Λ_h, the reorganization energy of electrons Λ_e, and the total reorganization energies Λ_{total} of the dyes*

	Λ_e(eV)	Λ_h(eV)	Λ_{total}(eV)
Dye-1	0.619	0.514	1.133
Dye-2	0.583	0.427	1.011
Dye-3	0.641	0.455	1.096

The Λ_h and the Λ_e were used to assess the charge injection and transfer capabilities of the hole transport materials. Total reorganization energy is used to calculate the total charge transfer between the donor and acceptor regions of a molecule. Reorganization energy is the term for the change in system energy that results from structural relaxation following an electron gain or loss. Charge transport benefits from a low reorganization energy. In Table 7, the value of Λ_{total} is in the following order: 1.133 (Dye-1) > 1.096 (Dye-3) > 1.011 (Dye-2), which indicates that Dye-2 is advantageous for transporting charges in the design.

3.8. Intramolecular Charge Transfer (ICT)

Typically, the optimal scenario involves the transfer of one electron from the donor unit to the acceptor unit upon activation. The state of effective charge separation can be expedited due to the favorable photoinduced ICT. To assess the amount of ICT, several important metrics are computed, including the transferred charge (q_{CT}), the charge transferred distance (d_{CT}), H, and t [48]. A quantitative assessment of the charge transfer length can be made using the definition of d_{CT}, which specifies the spatial separation between the two barycenters of the density exhaustion $\rho_-(r) = \Delta\rho(r)$, if $\Delta\rho < 0$ and density improvement $\rho_+(r) = \Delta\rho(r)$, if $\Delta\rho > 0$ distributions following excitation.

Table 8. *Computed ICT parameters of the investigated dyes*

Dyes	[a]q_{CT}	[b]d_{CT}	[c]t	[d]H	
Dye-1	0.702	4.150	0.587	3.563	
Dye-2	0.731	4.203	0,627	3.576	
Dye-3	0.696	4.085	0.548	3.537	
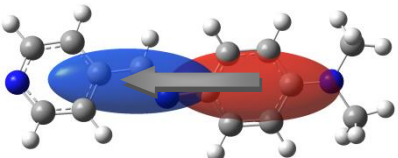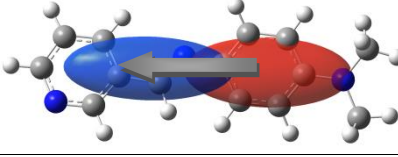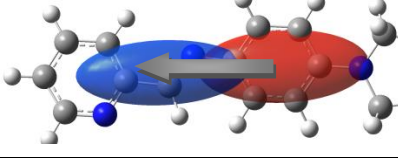
[a]$q_{CT}(ine^-)$:*The quantity of electrons transferred.*
[b]$d_{CT}(in\text{Å})$:*The duration of charge transfer.*
[c]$t(in\text{Å})$:*The degree to which electric charges are separated.*
[d]$H(in\text{Å})$:*The quantity being referred to is the average of the lengths of the centroid axis along the D-A direction.*

To conduct further research, we examined the ICT features. With the varying binding of the pyridine and the imine groups, as illustrated in Table 8, the H index (the half-sum of the centroid axis length along the D−A direction) changes only slightly. On the one hand, varying binding of the pyridine and imine groups can enhance Dye-2's H index, strengthening the hole and electron transfer. The highest H index value was achieved from Dye-2, although there is not much difference in the H index values. The connections of the pyridine group with the imine group in Dye-3 result in shortening of the dye's charge transfer d_{CT}, as seen in Table 8. The reduction of the E_{gap} is expected to result in a drop in d_{CT}. Compared to Dye-1, Dye-3's gap value rose by 0.068 eV, but its d_{CT} value reduced by 0.07 Å. A positive value for t (during the transfer of excitation charges from D to A) denotes a large charge separation and is a reasonable diagnostic indicator. All the t-values found were positive, as we expected. A lower molar extinction coefficient brought on by a fall in q_{CT} can affect device performance.

4. CONCLUSION

In brief, a comparative analysis has been conducted to investigate the impact of pyridine unit binding at various locations on the properties of DSSCs.

• At 443.52 nm, Dye-1 exhibited its strongest absorption peak, which was the highest among all the dyes. This absorption peak signifies the transition from the S_0 to S_1 excited state, created by electron transfer from HOMO to LUMO electronic transitions (70% configuration).

• Dye molecules with relatively modest frontier orbital gaps are frequently associated with low kinetic stability and high chemical reactivity. In comparison to the other dyes, Dye-1 is found to be the softest dye and exhibits strong chemical reactivity.

• The stabilization energy of Dye-1 was predicted at 2.530, indicating higher energy stability. Additionally, the ω value of Dye-1 was obtained at 0.980, showing that the largest electron-withdrawing ability among the dyes, thus having a stronger ability to attract electrons from the dye's acceptor moiety.

• The Light Harvesting Efficiency (LHE) values, ranging from 80.8 to 82.5, suggest that all dyes possess the capability to enhance the photocurrent response linked to the *f* of each dye molecule at the wavelength of maximum absorption.

• The calculated Δ_{Greg} values for Dye-1, Dye-2, and Dye-3 were 0.618 eV, 0.512 eV, and 0.461 eV, respectively. For DSSCs to achieve high efficiency, it is necessary to have a low regenerative driving force, as high propulsions can result in photovoltaic loss. According to this data, Dye-3 exhibits more suitable ΔG_{reg} values.

• We predicted Dye-1 would have a significant capacity for charge injection due to a stronger driving force, as Dye-1 has more negative computed ΔG^{inject} values. Therefore, we hypothesized that it would still demonstrate a significant load injection capacity. However, there is no assurance that the PCE of Dye-1 will rise

• We have conducted extensive research on the structure of the dyes and the functionality of the device, including the process of ICT of the dyes and the lifetime of the excited electrons. Our investigations serve as crucial references for subsequent experimental studies aiming to molecularly engineer pyridine-linked Schiff base molecules into highly effective DSSCs.

CONFLICTS OF INTEREST

No conflict of interest was declared by the authors.

REFERENCES

[1] Zheng, L., Cao, Q., Wang, J., Chai, Z., Cai, G., Ma, Z., Han, H., Li, Q., Li, Z., Chen, H., "Novel D–A−π–A-Type Organic Dyes Containing a Ladderlike Dithienocyclopentacarbazole Donor for Effective Dye-Sensitized Solar Cells", ACS Omega, 2(10): 7048-7056, (2017). https://doi.org/10.1021/acsomega.7b01387

[2] Ren, Y., Zhang, D., Suo, J., Cao, Y., Eickemeyer, F. T., Vlachopoulos, N., Zakeeruddin, S. M., Hagfeldt, A., Grätzel, M., "Hydroxamic acid pre-adsorption raises the efficiency of cosensitized solar cells", Nature, 613(7942): 60-65, (2022). https://doi.org/10.1038/s41586-022-05460-z

[3] O'Regan, B., Grätzel, M., "A low-cost, high-efficiency solar cell based on dye-sensitized colloidal TiO2 films", Nature, 353(6346): 737-740, (1991). https://doi.org/10.1038/353737a0

[4] Xie, Y., Tang, Y., Wu, W., Wang, Y., Liu, J., Li, X., Tian, H.,Zhu, W. H., "Porphyrin Cosensitization for a Photovoltaic Efficiency of 11.5%: A Record for Non-Ruthenium Solar Cells Based on Iodine Electrolyte", Journal of the American Chemical Society, 137(44): 14055-14058, (2015). https://doi.org/10.1021/jacs.5b09665

[5] Higashino, T., Imahori, H., "Porphyrins as excellent dyes for dye-sensitized solar cells: recent developments and insights", Dalton Transactions, 44(2): 448-463, (2015). https://doi.org/10.1039/c4dt02756f

[6] Zhang, S., Yang, X., Numata, Y., Han, L., "Highly efficient dye-sensitized solar cells: progress and future challenges", Energy Environmental Science, 6(5): 1443, (2013). https://doi.org/10.1039/c3ee24453a

[7] Luo, J., Xu, M., Li, R., Huang, K. W., Jiang, C., Qi, Q., Zeng, W., Zhang, J., Chi, C., Wang, P., Wu, J., "N-Annulated perylene as an efficient electron donor for porphyrin-based dyes: enhanced Light-harvesting ability and high-efficiency Co(II/III)-Based dye-sensitized solar cells", Journal of the American Chemical Society, 136(1): 265-272, (2013). https://doi.org/10.1021/ja409291g

[8] Zhou, G., Pschirer, N., Schöneboom, J. C., Eickemeyer, F., Baumgarten, M., Müllen, K., "Ladder-type pentaphenylene dyes for dye-sensitized solar cells", Chemistry of Materials, 20(5): 1808-1815, (2008). https://doi.org/10.1021/cm703459p

[9] Erdogdu, M., Atilgan, A., Erdogdu, Y., Yildiz, A., "Flavonoid from hedera helix fruits: a promising new natural sensitizer for DSSCs", Journal of Photochemistry and Photobiology A: Chemistry, 448: 115288, (2024). https://doi.org/10.1016/j.jphotochem.2023.115288

[10] Erdoğdu, M., Atilgan, A., Erdogdu, Y., Yildiz, A., "Natural dyes extracted from Ligustrum vulgare, Juniperus sabina, and Papaver rhoeas for novel DSSC applications", Materials Letters, 358: 135811 (2024). https://doi.org/10.1016/j.matlet.2023.135811

[11] Akdogan, N., Alp, M., Atilgan, A., Disli, A., Erdogdu, Y., Yildiz, A., "An AZO dye with nitril anchoring to dye-sensitized solar cell performance: A theoretical and experimental investigation", Materials Letters, 351: 135075, (2023). https://doi.org/10.1016/j.matlet.2023.135075

[12] Akdogan, N., Ortatepe, B., Atli, A., Disli, A., Erdogdu, Y., Yildiz, A., "A joint theoretical and experimental study on a tetrazole-anchored BODIPY-Based dye at the surface of TiO2 for Dye-sensitized solar cell applications", Physica Status Solidi (A), 2300513, (2023). https://doi.org/10.1002/pssa.202300513

[13] Nazeeruddin, M. K., Péchy, P., Renouard, T., Zakeeruddin, S. M., Humphry-Baker, R., Comte, P., Liska, P., Cevey, L., Costa, E., Shklover, V., Spiccia, L., Deacon, G. B., Bignozzi, C. A., Grätzel, M., "Engineering of efficient panchromatic sensitizers for nanocrystalline TiO2-Based solar cells", Journal of the American Chemical Society, 123(8): 1613-1624, (2001). https://doi.org/10.1021/ja003299u

[14] Liang, M., Chen, J., "Arylamine organic dyes for dye-sensitized solar cells", Chemical Society Reviews, 42(8): 3453, (2013). https://doi.org/10.1039/c3cs35372a

[15] Katoh, R., Furube, A., Yoshihara, T., Hara, K., Fujihashi, G., Takano, S., Murata, S., Arakawa, H., Tachiya, M., "Efficiencies of electron injection from excited N3 Dye into Nanocrystalline Semiconductor (ZrO2, TiO2, ZnO, Nb2O5, SnO2, In2O3) Films", The Journal of Physical Chemistry B, 108(15): 4818-4822, (2004). https://doi.org/10.1021/jp031260g

[16] Nicksonsebastin, D., Pounraj, P., Prasath, M., "Donor functionalized perylene and different π-spacer based sensitizers for dye-sensitized solar cell applications - a theoretical approach", Journal of Molecular Modeling, 28(4): (2022). https://doi.org/10.1007/s00894-022-05087-x

[17] Ooyama, Y., Inoue, S., Asada, R., Ito, G., Kushimoto, K., Komaguchi, K., Imae, I.,Harima, Y., "Dye-sensitized solar cells based on a novel fluorescent dye with a pyridine ring and a pyridinium dye with the pyridinium ring forming strong interactions with nanocrystalline tio2 films", European Journal of Organic Chemistry, 1: 92-100, (2009), https://doi.org/10.1002/ejoc.200900983

[18] Koumura, N., Wang, Z. S., Mori, S., Miyashita, M., Suzuki, E.,Hara, K., "Alkyl-Functionalized organic dyes for efficient molecular photovoltaics", Journal of the American Chemical Society, 128(44): 14256-14257, (2006). https://doi.org/10.1021/ja0645640

[19] Lee, M. J., Seo, K. D., Song, H. M., Kang, M. S., Eom, Y. K., Kang, H. S.,Kim, H. K., "Novel D-π-A system based on zinc-porphyrin derivatives for highly efficient dye-sensitised solar cells", Tetrahedron Letters, 52(30): 3879-3882, (2011). https://doi.org/10.1016/j.tetlet.2011.05.074

[20] Wang, Z., Cui, Y., Hara, K., Dan-oh, Y., Kasada, C., Shinpo, A., "A high-light-harvesting-efficiency coumarin dye for stable dye-sensitized solar cells", Advanced Materials, 19(8): 1138-1141, (2007). https://doi.org/10.1002/adma.200601020

[21] Zeng, W., Cao, Y., Bai, Y., Wang, Y., Shi, Y., Zhang, M., Wang, F., Pan, C., Wang, P., "Efficient dye-sensitized solar cells with an organic photosensitizer featuring orderly conjugated ethylenedioxythiophene and dithienosilole blocks", Chemistry of Materials, 22(5): 1915-1925, (2010). https://doi.org/10.1021/cm9036988

[22] Ayaz, M., Gündoğdu, Aytaç, S., Erdem, B., Çiftçi, H., Erdogdu, Y., "Microwave-assisted synthesis, characterizations, antimicrobial activities, and DFT studies on some pyridine derived Schiff bases", Journal of Molecular Structure, 1269: 133791, (2022). https://doi.org/10.1016/j.molstruc.2022.133791

[23] Frisch, M.J., et.al. Gaussian 09. Revision C.01; Gaussian, Inc.: Wallingford CT, 2009

[24] Becke, A. D., "Density-functional exchange-energy approximation with correct asymptotic behavior", Physical Review A, 38(6): 3098-3100, (1988). https://doi.org/10.1103/physreva.38.3098

[25] Becke, A. D., "Density-functional thermochemistry. III. The role of exact exchange", The Journal of Chemical Physics, 98(7): 5648-5652, (1993). https://doi.org/10.1063/1.464913

[26] Lee, C., Yang, W.,Parr, R. G., "Development of the Colle-Salvetti correlation-energy formula into a functional of the electron density", Physical Review B, 37(2): 785-789, (1988). https://doi.org/10.1103/physrevb.37.785

[27] Casanova, D., Rotzinger, F. P., Grätzel, M., "Computational study of promising organic dyes for high-performance sensitized solar cells", Journal of Chemical Theory and Computation, 6(4): 1219-1227, (2010). https://doi.org/10.1021/ct100069q

[28] Meng, S., Kaxiras, E., Nazeeruddin, M. K., Grätzel, M., "Design of dye acceptors for photovoltaics from first-principles calculations", The Journal of Physical Chemistry C, 115(18): 9276-9282, (2011). https://doi.org/10.1021/jp201646q

[29] Arunkumar, A., Shanavas, S., Anbarasan, P. M., "First-principles study of efficient phenothiazine-based D–π–A organic sensitizers with various spacers for DSSCs", Journal of Computational Electronics, 17(4): 1410-1420, (2018). https://doi.org/10.1007/s10825-018-1226-5

[30] Yanai, T., Tew, D. P., Handy, N. C., "A new hybrid exchange–correlation functional using the Coulomb-attenuating method (CAM-B3LYP)", Chemical Physics Letters, 393(1-3): 51-57, (2004). https://doi.org/10.1016/j.cplett.2004.06.011

[31] Zhao, Y., Truhlar, D. G., "The M06 suite of density functionals for main group thermochemistry, thermochemical kinetics, noncovalent interactions, excited states, and transition elements: two new functionals and systematic testing of four M06-class functionals and 12 other functionals", Theoretical Chemistry Accounts, 120(1-3): 215–241, (2007). https://doi.org/10.1007/s00214-007-0310-x28

[32] Chai, J. D., Head-Gordon, M., "Long-range corrected hybrid density functionals with damped atom–atom dispersion corrections", Physical Chemistry Chemical Physics, 10(44): 6615, (2008). https://doi.org/10.1039/b810189b

[33] Marinado, T., Nonomura, K., Nissfolk, J., Karlsson, M. K., Hagberg, D. P., Sun, L., Mori, S., Hagfeldt, A., "How the Nature of Triphenylamine-Polyene Dyes in Dye-Sensitized Solar Cells Affects the Open-Circuit Voltage and Electron Lifetimes", Langmuir, 26(4): 2592-2598, (2009). https://doi.org/10.1021/la902897z

[34] Pearson, R. G., "Absolute electronegativity and hardness: application to inorganic chemistry", Inorganic Chemistry, 27(4): 734-740, (1988), https://doi.org/10.1021/ic00277a030

[35] Nalwa, H. S., "Handbook of Advanced Electronic and Photonic Materials and Devices: Semiconductor devices", (2001).

[36] Erdogdu Y., Erkoc S., "Structural and Electronic Properties of Ti Doped Aluminum Clusters: Density Functional Theory Calculations", Journal of Computational and Theoretical Nanoscience, 9(6): 837-850, (2012), https://doi.org/10.1166/jctn.2012.2105.

[37] Domingo, L., Ríos-Gutiérrez, M., Pérez, P., "Applications of the Conceptual Density Functional Theory Indices to Organic Chemistry Reactivity", Molecules, 21(6): 748, (2016). https://doi.org/10.3390/molecules21060748

[38] Gázquez, J. L., Cedillo, A.,Vela, A., "Electrodonating and Electroaccepting Powers", The Journal of Physical Chemistry A, 111(10): 1966-1970,(2007), https://doi.org/10.1021/jp065459f.

[39] Berlin, Y. A., Hutchison, G. R., Rempala, P., Ratner, M. A., Michl, J., "Charge Hopping in Molecular Wires as a Sequence of Electron-Transfer Reactions", The Journal of Physical Chemistry A, 107(19): 3970-3980, (2003). https://doi.org/10.1021/jp034225i

[40] Foster, M. E., Wong, B. M., "Nonempirically tuned range-separated DFT accurately predicts both fundamental and excitation gaps in DNA and RNA nucleobases", Journal of Chemical Theory and Computation, 8(8): 2682-2687, (2012). https://doi.org/10.1021/ct300420f

[41] El Mouhi, R., Daoui, O., Fitri, A., Benjelloun, A. T., El Khattabi, S., Benzakour, M., Kurban, M. "A strategy to enhance V OC of π-conjugated molecules based on thieno [2, 3-b] indole for applications in bulk heterojunction organic solar cells using DFT, TD-DFT, and 3D-QSPR modeling studies", New Journal of Chemistry, 47(2): 812-827, (2023). https://doi.org/10.1039/D2NJ04281A

[42] Gündüz, B., Kurban, M., "Photonic, spectroscopic properties and electronic structure of PTCDI-C8 organic nanostructure", Vibrational Spectroscopy, 96: 46-51, (2018). https://doi.org/10.1016/j.vibspec.2018.02.008

[43] Kurban, M., Gündüz, B., Göktaş, F., "Experimental and theoretical studies of the structural, electronic and optical properties of BCzVB organic material", Optik, 182: 611-617, (2019), https://doi.org/10.1016/j.ijleo.2019.01.080

[44] Lu, T.,Chen, F., "Multiwfn: A multifunctional wavefunction analyzer", Journal of Computational Chemistry, 33(5): 580-592, (2011). https://doi.org/10.1002/jcc.22885

[45] Boschloo, G., Hagfeldt, A., "ChemInform abstract: characteristics of the iodide/triiodide redox mediator in dye-sensitized solar cells", ChemInform, 41(17): (2010), https://doi.org/10.1002/chin.201017268

[46] Wenger, S., Bouit, P. A., Chen, Q., Teuscher, J., Censo, D. D., Humphry-Baker, R., Moser, J. E., Delgado, J. L., Martín, N., Zakeeruddin, S. M., Grätzel, M., "Efficient electron transfer and sensitizer regeneration in stable π-extended tetrathiafulvalene-sensitized solar cells", Journal of the American Chemical Society, 132(14): 5164-5169, (2010). https://doi.org/10.1021/ja909291h

[47] Razavi, R., Kaya, S., Zahedifar, M., Ahmadi, S. A., "Simulation and surface topology of activity of pyrazoloquinoline derivatives as corrosion inhibitor on the copper surfaces", Scientific Reports, 11(1): (2021). https://doi.org/10.1038/s41598-021-91159-6

[48] Li, S., He, J., Jiang, H., Mei, S., Hu, Z., Kong, X., Yang, M., Wu, Y., Zhang, S., and Tan, H., "Comparative studies on the structure–performance relationships of phenothiazine-based organic dyes for dye-sensitized solar cells", ACS Omega, 6(10): 6817-6823, (2021). https://doi.org/10.1021/acsomega.0c05887